Rare Metal Materials and Engineering
Volume 55, Issue 3, March 2026
Available online at www.rmme.ac.cn

Science Press

Cite this article as: Zhao Yanchun, Yao Yatao, Zhang Fan, et al. Deformation Behavior and Mechanisms of fcc High-Entropy Alloys: Insights from Neutron Diffraction[J]. Rare Metal Materials and Engineering, 2026, 55(03): 655-664. DOI: https://doi.org/10.12442/j.issn.1002-185X.20250176.

REVIEW

Deformation Behavior and Mechanisms of fcc High-Entropy Alloys: Insights from Neutron Diffraction

Zhao Yanchun[1], Yao Yatao[1,2,3,4], Zhang Fan[4], Huang Yan[4], Zhang Yibo[4], Lu Zhichao[4], Zhang Qi[4], Fu Xiaoling[5], Wang Anding[6], Zhang Fei[2], Song Wenli[2,3], Ma Dong[4]

[1] State Key Laboratory of Advanced Processing and Recycling of Nonferrous Metals, School of Materials Science and Engineering, Lanzhou University of Technology, Lanzhou 730050, China; [2] Institute of High Energy Physics, Chinese Academy of Sciences (CAS), Bejing 100049, China; [3] Spallation Neutron Source Science Center, Dongguan 523803, China; [4] Neutron Science Center, Songshan Lake Materials Laboratory, Dongguan 523808, China; [5] School of Materials and Energy, Guangdong University of Technology, Guangzhou 510006, China; [6] Research Institute of Interdisciplinary Science, School of Materials Science and Engineering, Dongguan University of Technology, Dongguan 523808, China

Abstract: The multi-principal element characteristic of high-entropy alloys has revolutionized the conventional alloy design concept of single-principal element, endowing them with excellent mechanical properties. However, owing to this multi-principal element nature, high-entropy alloys exhibit complex deformation behavior dominated by alternating and coupled deformation mechanisms. Therefore, elucidating these intricate deformation mechanisms remains a key challenge in current research. Neutron diffraction (ND) techniques offer distinct advantages over traditional microscopic methods for characterizing such complex deformation behavior. The strong penetration capability of neutrons enables in-situ, real-time, and non-destructive detection of structural evolution in most centimeter-level bulk samples under complex environments, and ND allows precise characterization of lattice site occupations for light elements, such as C and O, and neighboring elements. This review discussed the principles of ND, experiment procedures, and data analysis. Combining with recent advances in the research about face-centered cubic high-entropy alloy, typical examples of using ND to investigate the deformation behavior were summarized, ultimately revealing deformation mechanisms dominated by dislocations, stacking faults, twinning, and phase transformations.

Key words: high-entropy alloys; neutron diffraction; face centered-cubic structure; deformation mechanism

1 Introduction

Based on the design concept of "multi-principal element" alloys[1–3], researchers have fabricated various high-entropy alloys (HEAs) with tunable crystal structures, which include face centered-cubic (fcc), body centered-cubic, and hexagonal close-packed (hcp) structures in single-phase or multi-phase forms[1–2,4], revealing an expansive design space for advanced alloys. Notably, many HEAs exhibit remarkable mechanical properties surpassing those of conventional alloys. For instance, fcc-structured HEAs based on Fe-Co-Cr-Ni-Mn systems exhibit superior fracture toughness at ambient temperature[5], high fatigue crack propagation thresholds[6], and exceptional resistance against low-temperature embrittlement even in cryogenic environments, such as liquid nitrogen (77 K) and liquid helium (4 K)[7–8]. In addition, micro-alloyed HEAs with a predominant fcc structure exhibit enhanced wear resistance, corrosion resistance, and comprehensive mechanical properties, achieving synergistic combinations of high strength and ductility[9–12]. These exceptional properties position fcc-structured HEAs as attractive candidates for aerospace components, energy systems, and engineering applications under extreme service conditions.

Received date: April 07, 2025
Foundation item: National Key R&D Program of China (2023YFB3711904, 2022YFA1603801); National Natural Science Foundation of China (12404230, 52471181, 52301213, 52130108, 52471005); National Nature Science Foundation of Zhejiang Province (LY23E010002); Open Fund of the China Spallation Neutron Source, Songshan Lake Science City (KFKT2023B11); Guangdong Basic and Applied Basic Research Foundation (2022A1515110805, 2024A1515010878)
Corresponding author: Song Wenli, Ph. D., Associate Researcher, Institute of High Energy Physics, Chinese Academy of Sciences (CAS), Beijing 100049, P. R. China, Tel: 0086-769-88931369, E-mail: songwl@ihep.ac.cn

The mechanical properties of materials are intrinsically correlated with their deformation mechanisms. In recent years, extensive investigations on the deformation mechanisms of HEAs have revealed that not only do they exhibit certain deformation modes similar to those of conventional alloys, but their distinctive compositional design engenders substantially more complex deformation behavior. A representative example is found in single-phase HEAs with fcc structure, where the stacking fault energy (SFE) serves as a pivotal parameter governing deformation mechanisms[13]. Substantial studies have established the following empirical correlations: when SFE exceeds 45 mJ/m^2, deformation is predominantly dominated by dislocation slip; when SFE is between 20–45 mJ/m^2, twinning-induced plasticity mechanism will be activated; when SFE is below 20 mJ/m^2, transformation-induced plasticity[14–16] occurs. However, the fundamental design of HEAs introduces unique characteristics, such as severe lattice distortion and sluggish diffusion effects, which significantly complicate their deformation mechanism. For instance, Wu et al[17] reported that severe lattice distortion in HEAs induces a weak yet non-negligible Labusch-type pinning effect on dislocation motion. Zhang et al[18] revealed that localized short-range ordered structures in NiCoCr alloy markedly increase the lattice friction stress for dislocation motion and modify their propagation channels, therefore profoundly influencing macroscopic mechanical properties. These intricate deformation phenomena promote the exceptional mechanical properties of HEAs, but simultaneously present considerable challenges for the comprehensive understanding of the deformation mechanisms.

Currently, the research on the deformation behavior and mechanism of HEAs considerably depends on transmission electron microscope (TEM) to observe the deformed microstructures. However, conventional ex-situ TEM can only permit observation of residual deformation structures at ambient conditions, which cannot capture the difference in microstructural evolution under varying environment or stress conditions. Furthermore, the restricted observation region (typically micron-scale) in in-situ TEM experiments cannot fully represent the deformation behavior of the bulk samples[19]. In contrast, neutron diffraction (ND) technique exhibits distinguished advantages for identifying deformation behavior in microstructural evolution of materials. (1) The penetration of neutrons in most metallic alloys reaches the centimeter scale, enabling non-destructive characterization of large bulk samples[20–21], and the diffraction information obtained by ND reflects the volume-averaged effect and has statistical significance due to three fundamental physical principles, as follows. 1) As electrically neutral particles, neutrons experience negligible electromagnetic interactions with electron clouds or atomic nuclei. 2) The internal structure of atoms is predominated by empty space, and the size of nucleus accounts for only about 10^{-15} of atom volume. Therefore, neutrons must directly collide with nuclei to be effectively scattered or absorbed. However, the probability of a neutron-nucleus collision event is extremely low. 3) The interaction force between neutron and nucleus shows no systematic variation with atomic number, maintaining strong penetration effect even through high atomic-number materials (such as Pb). This exceptional penetration effect ensures the in-situ investigation of the dynamic behavior of material under complex multi-field coupling environments[22–24]. (2) Neutron scattering intensities correlate with the nuclear scattering cross-sections rather than the atomic number. Therefore, it can be allowed to detect the signals of light elements (C, H, and O) of measurable concentrations and to statistically determine the lattice site occupancy of neighboring transition metals (Fe, Co, and Ni) [20–21]. Consequently, the in-situ ND technique provides real-time monitoring of complete structural evolution during plastic deformation, including crystal lattice parameter changes, defect accumulation of dislocations and stacking faults (SFs), light element content, and phase transformations, making it an effective method to study complex deformation behavior in HEAs.

This review discussed the fundamental principles, instrumentation configurations, and experiment data analysis of ND technique. Meanwhile, representative cases were used to demonstrate the unique advantages of ND in observing the complex deformation behavior in advanced materials with fcc structure. This review not only provides understanding of ND technique but also contributes to the application of ND technique in characterizing deformation mechanisms of structural materials.

2 Principles and Instrumentation of ND

X-ray diffraction obtains information through scattering by extranuclear electrons, whereas ND relies on direct interaction with atomic nuclei. However, ND also obeys Bragg's law $2d_{hkl}\sin\theta=n\lambda$, where d_{hkl} represents the lattice spacing of the (hkl) plane, 2θ denotes the diffraction angle, λ is the wavelength of the incident neutron beam, and n is the diffraction order. When neutrons undergo elastic coherent scattering with crystalline materials, diffraction peaks emerge exclusively at specific angles that satisfy the Bragg equation. The abscissa of the experimental diffraction spectrum can be characterized by the diffraction angle 2θ, lattice spacing d_{hkl}, or scattering vector $\boldsymbol{Q}$ ($|\boldsymbol{Q}|=4\pi\sin\theta/\lambda$), all of which are interrelated through the Bragg equation. The scattering vector $\boldsymbol{Q}$ attracts much attention. Bragg diffraction peaks dominate at higher $|\boldsymbol{Q}|$ values, reflecting the long-range ordered structure of the crystal. In contrast, when the $|\boldsymbol{Q}|$ value is extremely low (<0.1 nm^{-1}), weak diffusion scattering peaks usually appear, indicating spatial inhomogeneity in the system, such as nanoscale structural fluctuations or defect distributions[20]. By analyzing different $\boldsymbol{Q}$ regions, ND can resolve multiscale structural information spanning from atomic to mesoscopic, even macroscopic length scale. Therefore, this technique can provide a unique approach to investigate the lattice structures, defects, light elements of a certain amount, phase evolution, and other structural characteristics in materials.

The characterization of deformation behavior of structural material is generally conducted through engineering material

diffractometers of neutron sources. These instruments provide not only high-quality neutron beams but also versatile environments to accommodate diverse experimental requirements. Unlike reactor-based neutron sources that use constant-wavelength neutrons for sample interrogation, pulsed spallation neutron sources have emerged as a key platform to investigate the dynamic behavior and multiscale structures of complex materials, owing to their high pulse flux, broad energy spectrum coverage, exceptional time resolution, and enhanced safety[25]. The time-of-flight (TOF) method employed at spallation neutron sources is a diffraction technique based on the wavelength-time correlation characteristic of pulsed neutron beams. Its core principle is as follows: after the emission of neutron beam from the pulsed source, neutrons with different energies will have a time separation in the fixed-length flight paths due to the difference in their velocities (wavelength is inversely proportional to velocity). By precisely recording the arrival time of the neutrons that interact with the sample using high-resolution detectors, the corresponding wavelength can be calculated. Finally, combined with Bragg's diffraction law, the lattice parameters, phase composition, magnetic structure, and dynamic properties can be contained[26]. The spallation neutron source facility and the generation process of high-flux neutron beams are illustrated in Fig. 1[27], where high-energy protons are accelerated by linear accelerator and rapid circular synchrotron accelerator ring in cascade, and then they bombard a heavy metal target, inducing spallation reactions of the target nucleus and releasing a high-flux transient neutron beam. After the energy spectrum of the high-energy neutrons is moderated by the neutron moderator device, the high-energy neutrons are directionally transported to the sample position through a collimation guide tube. Finally, those neutrons undergo elastic/inelastic scattering with the sample and produce characteristic signals, which are captured by detector arrays and processed by electronic systems for data acquisition and recording. Among the major international spallation neutron sources, engineering material diffractometers, such as ENGIN-X at ISIS (UK), VULCAN at SNS (USA), and TAKUMI at J-PARC (Japan), have accumulated extensive datasets for in-situ characterization of engineering materials. Recently, the engineering material diffractometer at China Spallation Neutron Source (CSNS)[27] passed acceptance testing and commenced the trial operation stage. This milestone signifies that China has possessed the experimental capability for characterizing structural materials under varying temperature and stress conditions.

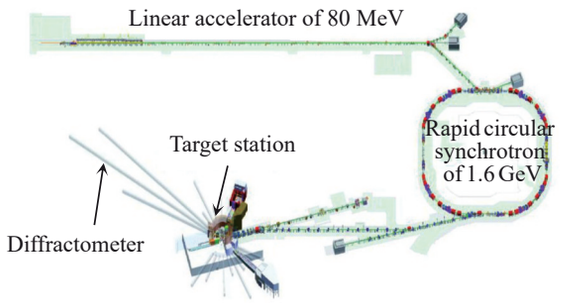

Fig.1 Device composition of accelerator-based spallation neutron source[27]

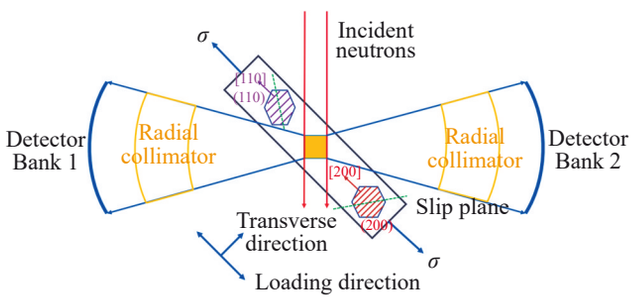

Fig.2 Schematic diagram of in-situ ND device[28]

3 In-situ Deformation ND Experiments and Data Processing

3.1 In-situ deformation ND experiments

The most commonly used experiment for ND to characterize the in-situ deformation behavior of structural materials is uniaxial tensile testing. The schematic diagram of the in-situ tensile experiment on the engineering material neutron diffractometer is shown in Fig.2[28]. By applying in-situ uniaxial tensile stress to the sample, both mechanical response curves and diffraction patterns at various strain levels can be acquired. During the elastic region, load-controlled deformation is typically implemented, whereas displacement control is adopted in the plastic region, i.e., the load is constant while the strain is progressively increased after yielding[28]. Engineering material neutron diffractometers are conventionally equipped with two primary detectors (±90°): Bank 1 and Bank 2, which are designed for simultaneous collection of diffraction data along the loading direction (LD) and the transverse direction (TD, direction perpendicular to LD), respectively. The lattice planes aligned with LD and TD are designated as (*hkl*)//LD and (*hkl*) ⊥TD, respectively. Under in-situ tensile conditions, the diffraction information of (*hkl*)//LD lattice planes more directly reflects the mechanical response of materials to applied stress. Consequently, researchers predominantly analyze (*hkl*)//LD diffraction data to elucidate the plastic deformation mechanisms of materials.

3.2 Analysis of in-situ deformation ND data

The original data obtained from in-situ deformation ND experiments are presented in Fig. 3[28]. Fig. 3b illustrates the variations in diffraction peaks from different (*hkl*)//LD during the deformation process of the material. As shown in Fig. 3b, the diffraction peak positions of (*hkl*)//LD gradually shift with the change of applied stress. Meanwhile, the diffraction intensities fluctuate due to defect formation and phase transition. Based on the information obtained from Fig. 3b, quantitative parameters, such as full width at half maximum

(FWHM), lattice strain, and peak intensity, can be extracted through single peak fitting and calculation through Rietveld refinement. These metrics enable precise characterization of real-time crystal structure evolution during the loading process, encompassing dislocation motion, SF source, and the phase transition onset[26,29–31], which thereby reveals the dynamic processes of material deformation. Furthermore, the elastic and plastic strains of (*hkl*)//LD or (*hkl*) ⊥TD with different orientations can be accurately calculated from peak position shifts, uncovering the deformation behavior of polycrystalline materials that depends on the grain orientation[8,32–33]. At the same time, by combining the macroscopic mechanical data (true stress-true strain curve) in Fig. 3a, the relationship between microstructure evolution and macroscopic mechanical properties can be established.

Based on the in-situ ND information, Rietveld refinement is conducted to obtain FWHM, peak position, and diffraction intensity of the diffraction peak. Currently, the mainstream refinement software includes Z-Rietveld for TAKUMI diffractometer[34] and VDRIVE for VULCAN diffractometer[35–37] along with the widely-used commercial packages, such as FullProf and GSAS-II[37–38].

As a predominant crystal defect during plastic deformation, dislocations induce lattice distortion effects, manifesting as diffraction peak broadening[7]. Unlike the systematic position shift of diffraction peaks caused by macroscopic stress, localized stress fields induce non-uniform lattice distortions in the sample to maintain mechanical equilibrium and lead to asymmetric broadening of diffraction peak profiles, which is a feature directly correlated with the spatial distribution of dislocation density. By integrating the related analysis methods, such as the Williamson-Hall refinement content and Krivoglaz-Wilkens dislocation theory[39], and determining the intrinsic parameters of the alloys, such as elastic constants and Burgers vector, the instrumental broadening contribution can be effectively subtracted, and the microstrain component is isolated. Based on a specific initial dislocation density distribution model, the strain-field-induced diffraction peak broadening effect can be quantitatively analyzed, enabling precise reconstruction of the dislocation density field distribution. By extracting FWHM parameter via the Rietveld whole-pattern-fitting method, semi-quantitative determination of dislocation density evolution can be achieved. Furthermore, combined with an in-depth analysis of the in-situ ND data using the convolutional multiple whole profile (CMWP) method, structural information, such as the dislocation type (edge/screw) and dislocation density evolution, can be analyzed[40–43]. This approach facilitates multiscale correlation between microstructure evolution and macroscopic plastic deformation mechanism. For example, Fig. 4 presents ND patterns of FeCoNiCrMn HEA obtained by CMWP method at strain of 26.0% and 52.6%[44]. The increasing dislocation density under different applied stress/strain confirms that the dislocation density changes with the change in stress/strain.

The lattice strain of grains with different orientations (ε_{hkl}) serves as a critical parameter for evaluating microstructure deformation. It can be calculated by $\varepsilon_{hkl}=(d_{hkl}-d^0_{hkl})/d^0_{hkl}$ [45] or $\varepsilon_{hkl}=(\mathrm{TOF}_{hkl}-\mathrm{TOF}^0_{hkl})/\mathrm{TOF}^0_{hkl}$ [7], where d_{hkl} is the lattice spacing of (*hkl*) planes under stress, d^0_{hkl} is the lattice spacing of stress-free sample, TOF_{hkl} is the Bragg position of (*hkl*) reflection under the stress state in TOF data, and TOF^0_{hkl} is the Bragg position under stress-free state. Fig. 5a–5c present the lattice strain-true stress curves of FeCoNiCrMn HEAs at different temperatures[7] using TOF data. It can be seen that the response for all (*hkl*) planes shows a linear change and the slope varies between different (*hkl*) planes in the elastic regime, reflecting the elastic anisotropy with different orientations. When the load-bearing capacity exceeds the upper limit, the curve begins to deviate from linearity, resulting in the fact that the crystal plane with this orientation enters the plastic deformation stage. At this time, the deformation also shows the characteristics of plastic anisotropy.

In fcc metals and alloys, the primary slip system occurs on (111) planes. Therefore, the intensity variation of the diffraction peaks is often used to serve as a critical indicator of dislocation slip activity[7,45]. The normalized peak intensity (I_{Nor}) is quantitatively expressed as $I_{\mathrm{Nor}}=I_{hkl}/I^0_{hkl}$, where I_{hkl} and I^0_{hkl} are the diffracted intensities under the stress and stress-free conditions, respectively. The evolution of I_{Nor}, namely the integrated intensity, with the variation of stress is demonstrated in Fig. 5d – 5f[7]. During the elastic stage, the integrated intensity barely changes; while in the plastic stage,

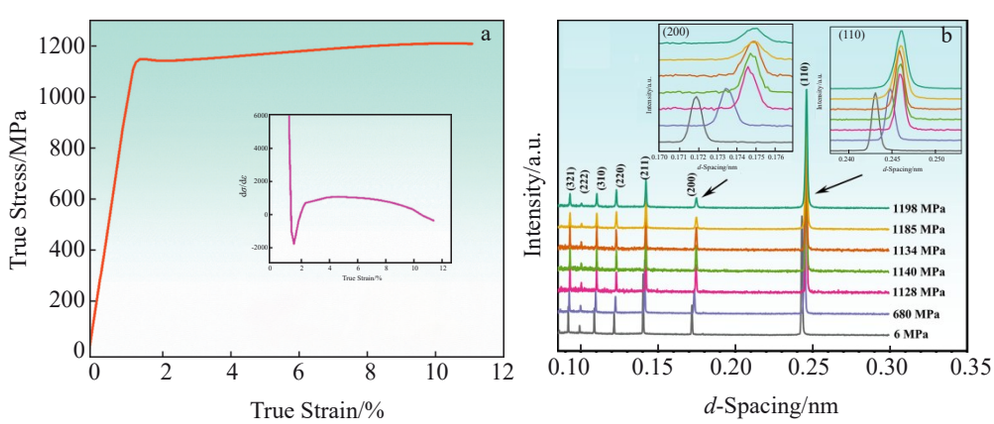

Fig.3 In-situ deformation ND data[28]: (a) true stress-true strain curve; (b) ND patterns

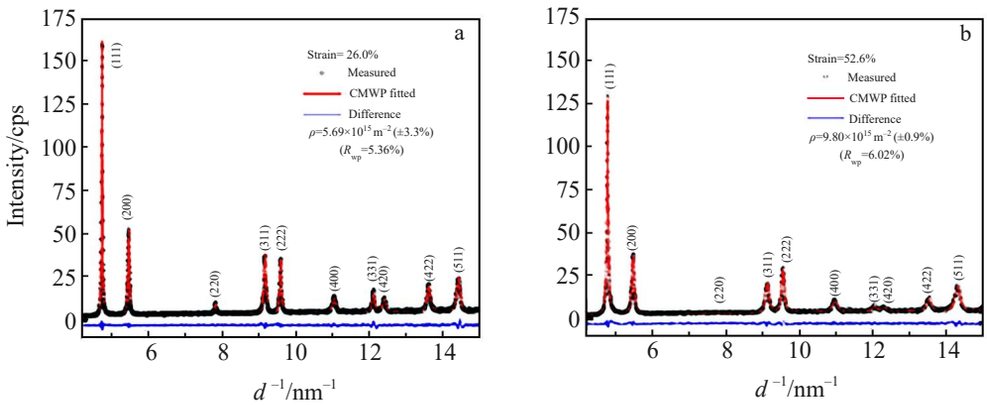

Fig.4 ND patterns of FeCoNiCrMn HEAs at 15 K under different strains[44]: (a) 26.0% and (b) 52.6%

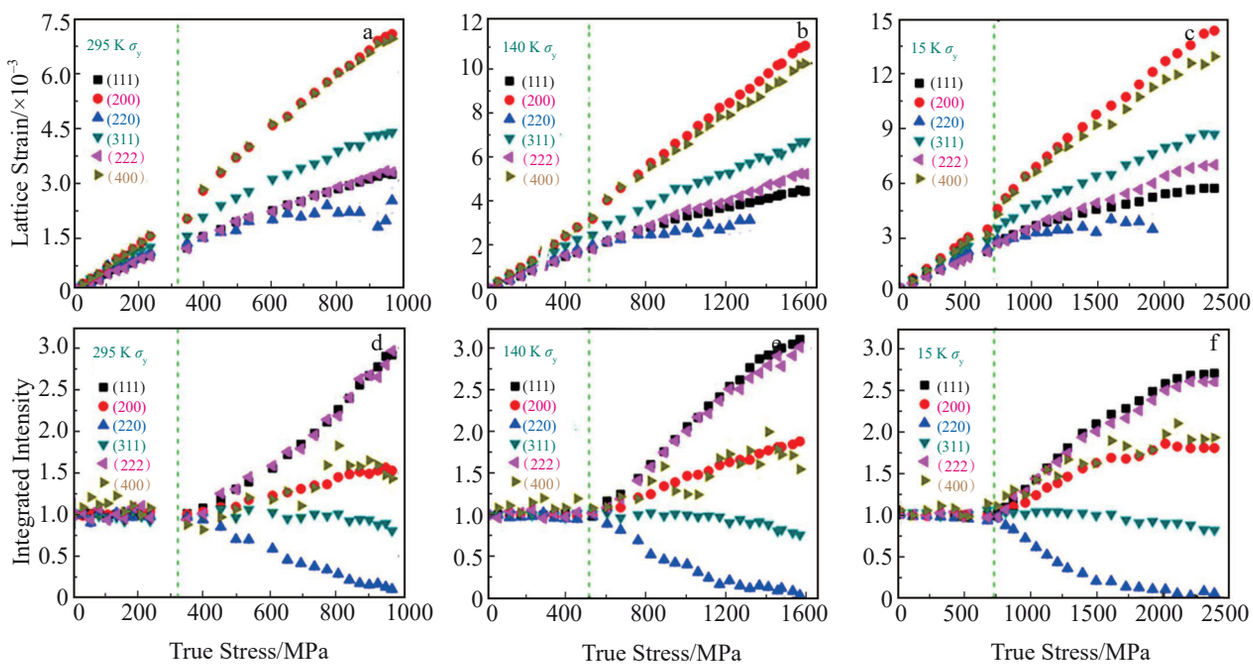

Fig.5 Lattice strain (a–c) and integrated intensity (d–f) results of FeCoNiCrMn HEAs at different temperatures[7]: (a, d) 295 K, (b, e) 140 K, and (c, f) 15 K

the integrated intensities of different (*hkl*) crystal planes exhibit either an increasing or decreasing trend. An increase in integrated intensity indicates that the grains preferentially rotate toward the (*hkl*) orientation under stress, such as (111) and (200). Conversely, a decrease in integrated intensity suggests that the grains with the (*hkl*) orientation rotate toward other orientations under stress.

The cross-scale collaborative analysis of TEM characterization with the aforementioned diffraction data enables systematic tracking of dynamic microstructure evolution involving dislocations, SFs, and other defects. This approach provides critical experiment evidence for establishing the structure-property relationship between micro-defects and macroscopic mechanical performance in fcc HEAs.

4 In-situ ND Investigation of Plastic Deformation Mechanisms in fcc HEAs

In-situ ND studies of deformation mechanisms have achieved considerable maturity in various material systems, including pure metals[46–47], superalloys[48–49], shape-memory alloys[50–51], and steels[52–55]. Recently, there have also been significant research breakthroughs in elucidating the intrinsic mechanisms underlying complex deformation behavior of HEAs through in-situ ND technique.

4.1 Dislocation-controlled deformation mechanisms

In the early development stages of HEAs, researchers speculated that the deformation behavior of typical fcc-structured HEAs, such as FeCoNiCrMn, would differ significantly from that of pure fcc metals due to their complex compositional characteristics. However, Wu et al[56] employed

in-situ ND and the Kröner model[57–59] to calculate the shear anisotropy value of FeCoNiCrMn HEA as 2.84, which is lower than that of ternary FeNiCr alloy (3.78) but close to that of pure fcc-Ni (2.51) [60–61]. Furthermore, its lattice strain evolution was similar to that of pure fcc metals[62], showing the mixed dislocations dominating the deformation behavior. These findings demonstrated that despite its complex composition, FeCoNiCrMn HEA exhibits deformation anisotropy and microstructure evolution comparable to those of pure metals and single-phase alloys. This study overturned the traditional concept of the deformation mechanisms of HEAs and laid a theoretical foundation for subsequent research. It is worth noting that Muhammad et al[7] conducted investigations on FeCoNiCrMn HEA at ambient temperature, and they also confirmed that dislocation slip controls the entire deformation process. Their systematic and innovative methods provided guiding insights for subsequent research. Additionally, element substitution strategies have been explored in the deformation mechanism studies of the series of FeCoNiCrMn HEAs. In Ref. [63 – 64], Mn was replaced with larger-radius elements, such as Pd and Cu. These representative studies revealed that the macroscopic stress-lattice strain curves obtained from in-situ ND deformation were similar to those of FeCoNiCrMn HEAs[7,56], showing dislocation slip as the dominant mechanism during plastic deformation.

Tang et al[65] used the changes in ND peaks to characterize dislocation behavior. They calculated the maximum dislocation densities of an FeCrNi alloy at 293 and 15 K using the CMWP method as 5.7×10^{14} and 7.9×10^{14} m^{-2}, respectively. These values are lower than the theoretical upper limit of dislocation density of fcc alloys (approximately 10^{18} m^{-2})[66–67]. The plasticity at 293 and 15 K is 40% and 19%, respectively. Combining the normalized intensity changes of diffraction peak (Fig. 6) with the theory proposed in Ref. [42], the lower plasticity at 15 K can be explained by the small-scale grain rotation and sluggish texture evolution, which confines the dislocation motion to preferentially activated slip planes, therefore restricting large-scale plastic deformation. Furthermore, fewer slip systems were activated in non-preferred deformation planes. At 15 K, the minor changes in intensity indicate that dislocation motion occurs only within a limited range, thereby preventing significant plastic deformation. This explanation aligns with the observed mechanical behavior and dislocation evolution.

4.2 SFs and deformation twinning mechanisms

First-principles calculations predict that the fcc phase can be transformed into hcp phase at low temperatures[68–69]. However, in-situ ND patterns revealed that the FeCoNiCrMn HEAs retained the fcc phase during deformation, even at 140 and 15 K[7]. The relationship between stress and lattice strain shows that with the decrease in temperature from 298 K to 140 K and further to 15 K, ε_{111} differs from ε_{222} during the plastic deformation stage, and their difference becomes more and more significant with the increase in stress. Similar phenomena also occur in terms of ε_{200} and ε_{400}. The reason is that (111) and (222) belong to the same crystallographic plane, so do (200) and (400). It is suggested that the splitting phenomenon causes the generation of SFs during deformation, and the increasing difference indicates a higher density of SFs. The stacking fault probability (SFP) is further quantified by $SFP=32\pi/3\sqrt{3}(\varepsilon_{<222>}-\varepsilon_{<111>})$ and $SFP=-32\pi/3\sqrt{3}(\varepsilon_{<400>}-\varepsilon_{<200>})$.

Based on the theoretical framework of SFP, the microstructure evolution during deformation was investigated by comparing SFP of ε_{111} and ε_{222} with integrated intensity of (111) plane as a function of stress, as illustrated in Fig. 7[7]. It can been seen that at room temperature, the integrated intensity of the (111) plane increases sharply during the plastic stage, whereas SFP shows no significant change, indicating that deformation is dominated by dislocation slip (stage 1–2 in Fig. 7). At 15 K, the increasing rate in diffraction peak intensity of the (111) plane is much slower than that at room temperature, which coincides with the significant rise in SFP due to extensive dissociation of perfect dislocations into SFs. This result suggests that subsequent work hardening is no longer dominated by dislocation propagation (stage 2 – 4 in Fig. 7). To further validate this conclusion, Naeem et al[44] fitted the dislocation densities at strain of 26.0% and 52.6% and temperature of 15 K, and the results were 5.69×10^{15} and 9.08×10^{15} m^{-2}, respectively. It was also found that the

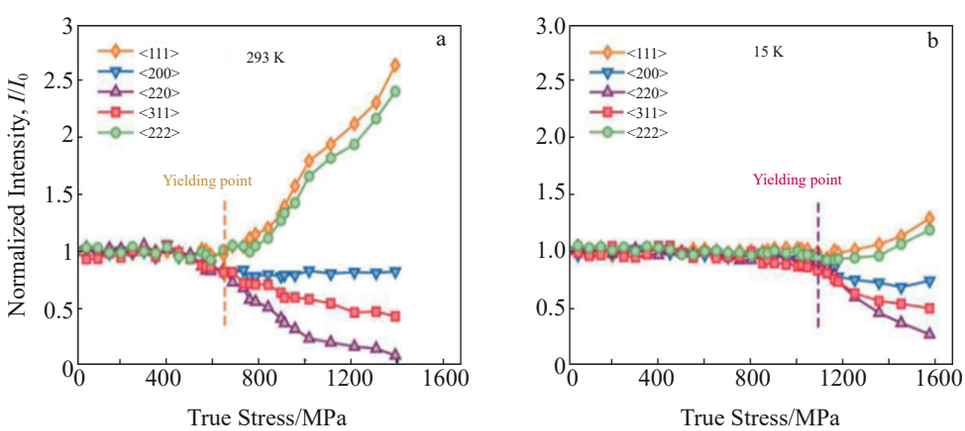

Fig.6 Evolution of normalized intensity of diffraction peaks of FeCrNi alloy at different temperatures[65]: (a) 293 K and (b) 15 K

dislocation density reached a saturation value once the strain reached 45%, which further supported the theory that SFs dominated subsequent deformation. In the final large-strain stage (after stage 4 in Fig.7), SFP continued to increase while the integrated intensity of the (111) plane stabilized, suggesting that deformation twinning might become the dominant mechanism. Although it was proposed that deformation twinning controlled the process according to the changes in SFP and integrated intensity, the evidence for deformation twinning was not as intuitive as that for SFs. Therefore, Naeem et al[44] examined the post-deformation microstructure using TEM. It was found that the deformed microstructure at room temperature was primarily composed of dislocations. Whereas at 15 K, the plastic deformation involved the collaborative activity of dislocations, SFs, and deformation twinning. TEM analysis provided direct evidence to support their interpretation of the deformation mechanisms in in-situ ND experiment.

Based on the twinning mechanism related to SFs[7], Shang et al[70] investigated the influence of the addition of light element C on the deformation mechanisms of NiCoCr alloys using in-situ ND. To be more specific, NiCoCr alloy was referred to as C_0, and $NiCoCrC_{0.75}$ alloy was referred to as $C_{0.75}$. It was revealed that the addition of C enhanced the overall lattice strain of the NiCoCr system, leading to maximum lattice strain of (111) plane as 0.0054 and 0.0070 for C_0 and $C_{0.75}$, respectively. To further understand the effect of C addition on the deformation mechanisms of NiCoCr system, the results of dislocation density, SFP, and twinning fault probability are shown in Fig.8. The results demonstrate that during deformation, the $C_{0.75}$ alloy exhibited higher dislocation density, critical strain values for the formation of SFs and twinning, as well as greater SFP and twinning fault probability, compared with those of the C_0 alloy. These findings indicate that the addition of C promotes the dislocation motion and multiplication. Subsequently, the high dislocation density facilitates the simultaneous formation of SFs and twinning during the intermediate deformation stage. The higher densities of SFs and twinning alleviate stress concentration, thereby enhancing strength while preserving the plastic deformation capability of the material.

Cai et al[71] investigated the effect of Mo microalloying on the deformation behavior of FeCoCrNi HEAs (ductility: 45%) using in-situ ND. Lattice strain analysis confirmed that deformation twinning, except dislocation slip, played a critical role in the plastic deformation of the as-extruded $FeCoCrNiMo_{0.23}$ HEAs (ductility: 53%). The activation of deformation twinning enhanced grain rotation and texture

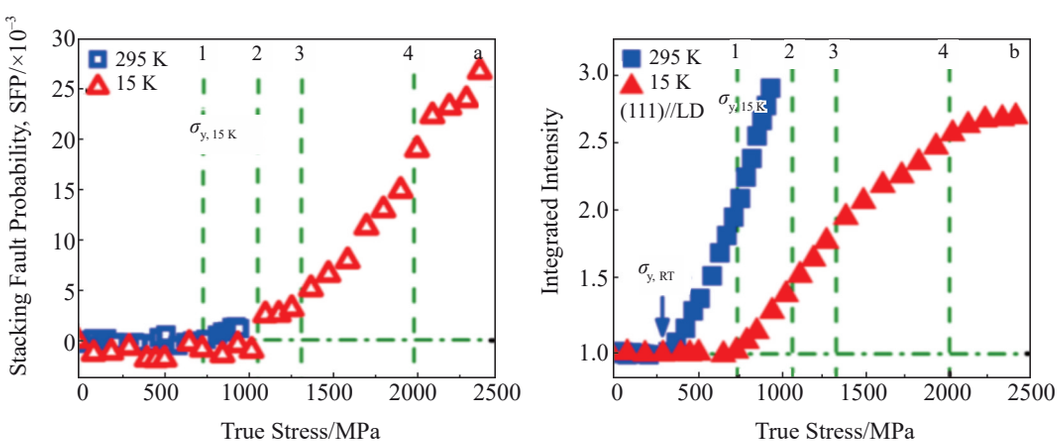

Fig.7 Evolution of SFP (a) and integrated intensity (b) of FeCoNiCrMn HEA[7]

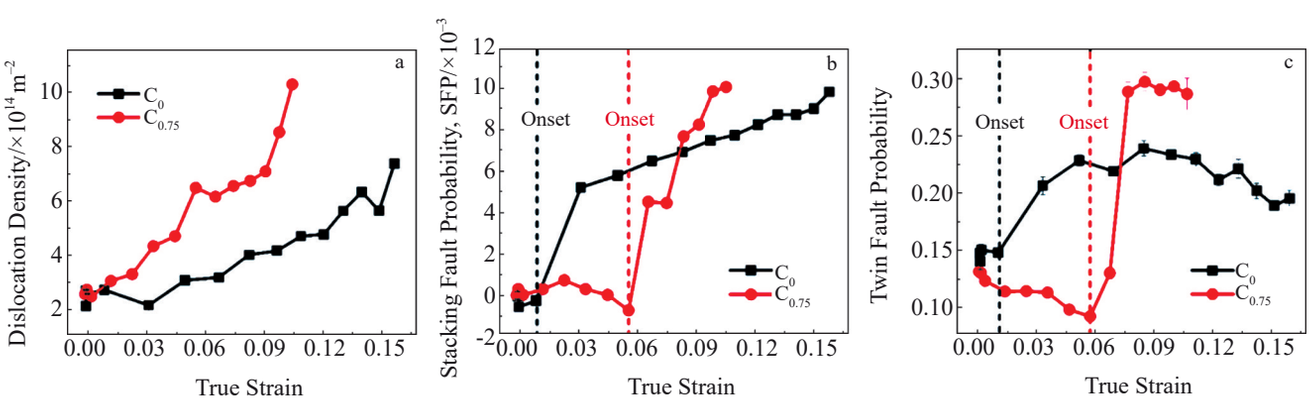

Fig.8 In-situ ND analysis results of C_0 and $C_{0.75}$ alloys[70]: (a) dislocation density; (b) SFP; (c) twinning fault probability

evolution in the as-extruded HEAs, thereby improving ductility. In contrast, the evolution of normalized diffraction intensity demonstrated that the annealed $FeCoCrNiMo_{0.23}$ HEAs (ductility: 13%) displayed restricted grain rotation and texture development, hindering the dislocation motion and ultimately leading to reduced plasticity.

4.3 Deformation mechanism dominated by phase transformation

In-situ ND enables the characterization of phase transformation behavior during material deformation by detecting changes in the intensity of characteristic (*hkl*) diffraction peaks and the emergence of new peaks that result from alterations in the crystal structure during phase transitions. Wei et al[72] conducted room-temperature in-situ ND studies. They revealed that compared with the $Co_{20}Cr_{20}Mn_{20}Ni_{20}Fe_{20}$ and $Co_{35}Cr_{20}Mn_{15}Ni_{15}Fe_{15}$ HEAs with higher SFEs, the $Co_{35}Cr_{25}Mn_{15}Ni_{15}Fe_{10}$ HEAs with an extremely low SFE (7.8 mJ/m^2) exhibited significant increase in localized SFs, as demonstrated by SFP calculations. Concurrently, numerical analysis of twinning fault probability indicated that the deformation twinning formed more readily, and it subsequently triggered an fcc-to-hcp phase transformation during further deformation, thereby markedly enhancing the work hardening capability. These findings provide direct experiment support for the theoretical framework.

Recently, He et al[73] employed in-situ ND to investigate the low-temperature phase transformation behavior of CrCoNi alloy. Fig.9a shows the in-situ ND patterns of CrCoNi alloy at 15 K, where the $hcp_{(101)}$ diffraction peak appears with the increase in stress. He et al[73] constructed the diagram based on the Shoji-Nishiyama orientation relationship[74] and the characteristic that the asymmetry of fcc diffraction peaks is the signature of intrinsic stacking faults (ISFs), suggesting that during plastic deformation stage II and III (Fig.9b), the peak intensity of $fcc_{(220)}\perp$TD decreases, the volume fraction of hcp phase increases, and SFP increases. However, the variation degree is less pronounced in stage II than that in stage III. Furthermore, based on the strong correlation between SFP and volume fraction of hcp phase, it was proposed that at the nanoscale, the nucleation of hcp phase is induced by ISFs, and the stable growth of hcp phase is accompanied by a sharp increase in SFs.

5 Conclusions and Future Perspectives

Owing to their outstanding mechanical properties, fcc HEAs have emerged as a focal point in material science. To reveal the intricate deformation mechanisms of HEAs, such as dislocation multiplication, SF activation, and the origins of fcc-to-hcp phase transition, in-situ ND has proven to be an irreplaceable technique. This powerful method enables real-time, non-destructive monitoring of lattice parameter changes, texture evolution, and phase transformation kinetics within fcc HEAs during deformation. At the atomic scale, ND provides crucial insights into the dynamic interactions among deformation mechanisms, thereby significantly advancing the understanding of the deformation mechanisms and guiding the rational design of high-performance fcc HEAs.

It is necessary to conduct further studies on combined test method involving ND and to continue developing data analysis methodologies for more accurate characterizations. The completion and operation of CSNS as well as improvement of neutron diffractometers suitable for different sample environments have provided strong support for the research on HEAs under multi-field coupling conditions. The application of ND to the studies of HEAs can not only promote the development and performance optimization of high-performance HEAs, but also provide useful information for the design of traditional materials, such as steels and superalloys.

On the one hand, the integration of ND and multiscale simulation has been a new trend to investigate the deformation mechanisms in other alloy systems. For instance, Voothaluru et al[75] combined crystal plasticity finite element modeling with in-situ ND experiments to investigate the lattice strain response of austenite and martensite phases, providing theoretical insights for the improvement of the fatigue life and reliability of bearings. Nycz et al[76] integrated ND-based residual stress measurement with a thermo-mechanical finite element model in ABAQUS software, establishing an efficient

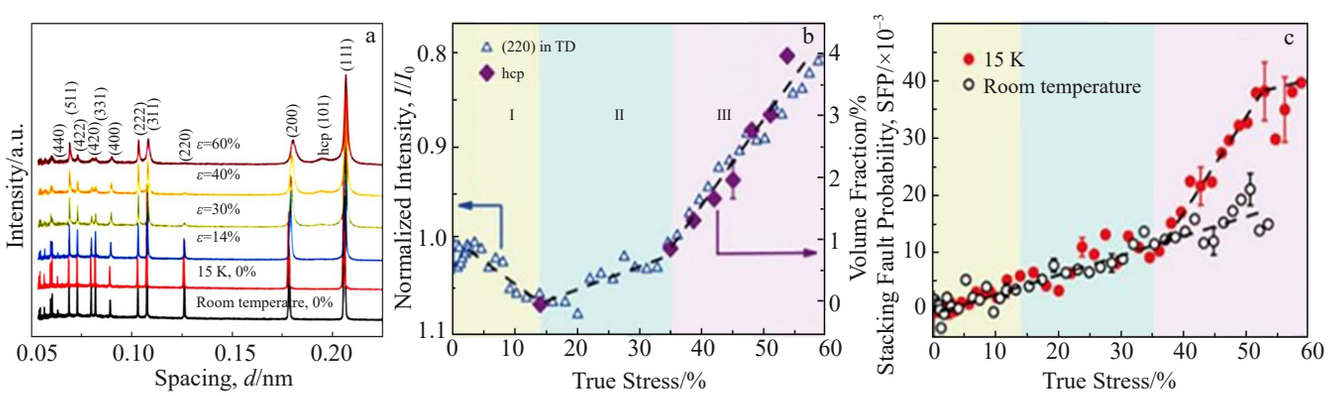

Fig.9 Analysis results of CoCrNi alloy[73]: (a) in-situ ND patterns after deformation at 15 K; (b) normalized intensity of $fcc_{(220)}\perp$TD diffraction peaks and hcp volume fraction as a function of true strain; (c) evolution of SFP with true strain at room temperature and 15 K

residual stress prediction framework. The developed residual stress prediction method offers an effective analytical tool to optimize the process parameters in large-scale metal additive manufacturing. As a contrast, such research in fcc HEAs is rare. Therefore, in the future, it is necessary to strengthen the integration of ND technique and multiscale simulations to establish a more complete framework to understand the complex deformation behavior of HEAs.

On the other hand, the developed fcc alloys can also be further investigated using ND, and existing ND methodologies can provide theoretical guidance for subsequent fcc HEA studies. For instance, a laser-remelted FeCrAlCu(Ni, Co) HEAs coating with excellent wear resistance can be fabricated[77]. ND can be employed to further analyze its residual stress, strain distribution, interfacial diffusion behavior, and even tensile deformation behavior in small-sized samples. Dong et al[78] measured the circumferential strain in the weld zone and adjacent regions on the (110) crystal plane of a beryllium ring using ND, establishing a methodological foundation for subsequent residual stress testing in HEAs. Multiple studies have demonstrated that spallation neutron techniques can effectively reveal dynamic processes in additive manufacturing, including metallurgical reactions, defect formation, and microstructure evolution within transient molten pools, making this approach a promising method for additive-manufactured HEAs[79]. This review summarized abundant research objects for in-situ ND investigations, offering development pathway for neutron-based research.

References

1 Yeh J W, Chen S K, Lin S J *et al*. *Advanced Engineering Materials*[J], 2004, 6(5): 299
2 Cantor B, Chang I T H, Knight P *et al*. *Materials Science and Engineering A*[J], 2004, 375–377: 213
3 Yeh J W. *Annales de Chimie Science des Matériaux*[J], 2006, 31(6): 633
4 George E P, Raabe D, Ritchie R O. *Nature Reviews Materials*[J], 2019, 4(8): 515
5 Gludovatz B, Hohenwarter A, Cantor D *et al*. *Science*[J], 2014, 345(6201): 1153
6 Gludovatz B, Hohenwarter A, Thurston K V S *et al*. *Nature Communication*[J], 2016, 7: 10602
7 Muhammad N H H, Zhang F, Wang X L *et al*. *Science Advances*[J], 2020, 6(13): 308
8 Tang L, Yan K, Cai B *et al*. *Scripta Materialia*[J], 2020, 178: 166
9 Liu X T, Lei W B, Ma L J *et al*. *Rare Metal Materials and Engineering*[J], 2016, 45(9): 2201
10 Zhao C M, Wu H, Zhang J F *et al*. *Rare Metal Materials and Engineering*[J], 2021, 50(8): 2783
11 Zhao Y C, Song H Z, Ma H W *et al*. *Rare Metal Materials and Engineering*[J], 2024, 53(7): 1817
12 Feng Li, Wang Zhipeng, Zhao Yanchun *et al*. *Rare Metal Materials and Engineering*[J], 2024, 53(11): 3175 (in Chinese)
13 Jo M, Koo Y M, Lee B J *et al*. *Applied Physical Sciences*[J], 2014, 111(18): 6560
14 Huang S, Li W, Lu S. *Scipta Materialia*[J], 2015, 108: 44
15 Tirunilai A S, San J, Weiss K P *et al*. *Journal of Materials Research*[J], 2018, 33: 3287
16 Li Z, Tasan C C, Pradeep K G *et al*. *Acta Materialia*[J], 2017, 131: 323
17 Wu Z, Gao Y, Bei H. *Acta Materialia*[J], 2016, 120: 108
18 Zhang R, Zhao S, Minor A M *et al*. *Nature*[J], 2020, 581(7808): 283
19 Bu Y, Wu Y, Lei Z *et al*. *Nature Communication*[J], 2024, 15: 4599
20 Wang Yanxu, Gong Wu, Sun Yuhua *et al*. *Acta Metallurgica Sinica*[J], 2024, 60(8): 1001 (in Chinese)
21 Shi Jindong, Geng Changjian, Xing Pichen *et al*. *Aeroengine*[J], 2020, 46(3): 59 (in Chinese)
22 Park M J, Yang H N, Jang D Y *et al*. *Journal of Materials Processing Technology*[J], 2004, 155–156: 1171
23 Dutta M, Bruno G, Edwards L *et al*. *Acta Materialia*[J], 2004, 52(13): 3881
24 Paradowska A, Price J W H, Ibrahim R *et al*. *Journal of Materials Processing Technology*[J], 2005, 164–165: 1099
25 Yu X, Cheng Y, Li Y *et al*. *Chemical Reviews*[J], 2023, 123(13): 8638
26 Malamud F, Santisteban J R, Vicente M A *et al*. *Journal of Applied Crystallography*[J], 2014, 47(4): 1337
27 Wang Sheng, Fu Shinian, Qu Huaming *et al*. *Atomic Energy Science and Technology*[J], 2022, 59(6): 1748 (in Chinese)
28 Zhou Y, Song W, Zhang F *et al*. *Journal of Alloys and Compounds*[J], 2024, 971: 172635
29 Sasaki T, Takahashi S, Kanematsu Y *et al*. *Wear*[J], 2008, 265(9–10): 1402
30 Daymond M R, Preuss M, Clausen B. *Acta Materialia*[J], 2007, 55(9): 3089
31 Clausent T L B. *Acta Materialia*[J], 1998, 46(9): 3087
32 Wei B, Wang L, Zhang Y. *Acta Materialia*[J], 2022, 225: 117571
33 Kwon H, Sathiyamoorthi P, Gangaraju M K *et al*. *Acta Materialia*[J], 2023, 248: 11881
34 Oishi R, Yonemura M, Nishimaki Y *et al*. *Nuclear Instruments and Methods in Physics Research Section A: Accelerators, Spectrometers, Detectors and Associated Equipment*[J], 2009, 600(1): 94
35 Lyu Z, Liu C, Xie D *et al*. *Intermetallics*[J], 2024, 168: 108241
36 He H, Wang B, Ma D *et al*. *Intermetallics*[J], 2021, 139: 107371
37 Yu C, Lin K, Zhang Q *et al*. *Nature Communication*[J], 2024, 15: 2252
38 Toby B H. *Journal of Applied Crystallography*[J], 2001, 34(2): 210
39 Mikhail A K, Leonid V A. *Theory of X-ray and Thermal Neutron Scattering by Real Crystals*[M]. New York: Plenum Press, 1969
40 Lee T H, Shin E, Oh C S *et al*. *Acta Materialia*[J], 2010, 58(8): 3173
41 Ribárik G, Gubicza J, Ungár T *et al*. *Materials Science and Engineering A*[J], 2004, 387–389: 343
42 Marc A M, Krishan K C. *Mechanical Behavior of Materials*[M]. Cambridge: Cambridge University Press, 2009
43 Gábor R. *Modeling of Diffraction Patterns Based on Microstructural Properties*[D]. Budapest: Eötvös Loránd

University, 2008
44 Naeem M, He H, Harjo S *et al*. *Scripta Materialia*[J], 2020, 188: 21
45 Stoica G M, Stoica A D, Miller M K *et al*. *Nature Communication*[J], 2014, 5: 5178
46 Zheng R, Gong W, Du J P *et al*. *Acta Materialia*[J], 2022, 238: 118243
47 Lee M S, Kawasaki T, Yamashita T *et al*. *Scientific Reports*[J], 2022, 12(1): 3719
48 Gao Y, Ding Y, Li L *et al*. *Intermetallics*[J], 2021, 138: 107340
49 Yang J, Li H, Gao T *et al*. *Journal of Alloys and Compounds*[J], 2024, 977: 173382
50 Li H, Yang Z, Shen H *et al*. *Acta Materialia*[J], 2023, 247: 118737
51 Wang Z, Chen J, Besnard C *et al*. *Materials Letters*[J], 2020, 281: 128676
52 He S H, He B B, Zhu K Y *et al*. *Scripta Materialia*[J], 2019, 168: 23
53 Wang Y, Tomota T, Ohmura T *et al*. *Acta Materialia*[J], 2020, 184: 30
54 Lin S, Borgenstam A, Stark A *et al*. *Materials Characterization* [J], 2022, 185: 111774
55 Li L, Miyamoto G, Zhang Y *et al*. *Journal of Materials Science & Technology*[J], 2024, 184: 221
56 Wu Y, Liu W H, Wang X L *et al*. *Applied Physics Letters*[J], 2014, 104(5): 051910
57 András B, Juliana D, Gábor R *et al*. *Journal of Applied Crystallography*[J], 2003, 36(1): 160
58 Ng E J, Hong V A, Yang Y *et al*. *Journal of Microelectromechanical Systems*[J], 2015, 24(3): 730
59 Ungár T, Dragomir I, Révész Á *et al*. *Journal of Applied Crystallography*[J], 1999, 32(5): 992
60 Ledbetter H M. *Physica Status Solidi (a)*[J], 1984, 85(1): 89
61 Wang Y, Huang H Y, Xie J X. *Materials Science and Engineering A*[J], 2011, 530: 418
62 Neil C J, Wollmershauser J A, Clausen B *et al*. *International Journal of Plasticity*[J], 2010, 26(12): 1772
63 Ying H, Yang X, He H *et al*. *Scripta Materialia*[J], 2024, 250: 116181
64 Amalia L, Li Y, Bei H *et al*. *Applied Physics Letters*[J], 2024, 124(14): 141901
65 Tang L, Jiang F Q, Wróbel J S *et al*. *Journal of Materials Science & Technology*[J], 2022, 116: 103
66 Cotterill R M J. *Physics Letters A*[J], 1977, 60(24): 61
67 Essmann U, Mughrabi H. *Philosophical Magazine A*[J], 2006, 40(6): 731
68 Huang S, Li W, Lu S *et al*. *Scripta Materialia*[J], 2015, 108: 44
69 Tian F, Varga L K, Shen J *et al*. *Science*[J], 2016, 111: 350
70 Shang Y Y, Wu Y, He J Y *et al*. *Intermetallics*[J], 2019, 106: 77
71 Cai B, Liu B, Kabra S *et al*. *Acta Materialia*[J], 2017, 127: 471
72 Wei D, Gong W, Tsuru T *et al*. *International Journal of Plasticity* [J], 2022, 158: 103117
73 He H, Naeem M, Zhang F *et al*. *Nano Letters*[J], 2021, 21(3): 1419
74 Nishiyama Z. *Martensite to Martensitic Transformation*[M]. New York: Academic Press, 1978
75 Voothalurua R, Bedekara V, Xie Q *et al*. *Materials Science and Engineering A*[J], 2018, 711: 579
76 Nycz A, Lee Y, Noakes M *et al*. *Materials & Design*[J], 2021, 205: 109751
77 Ma K, Feng L, Zhao Y C *et al*. *Rare Metal Materials and Engineering*[J], 2024, 53(10): 2747
78 Dong Ping, Wang Hong, Li Jian *et al*. *Rare Metal Materials and Engineering*[J], 2016, 45(12): 3197 (in Chinese)
79 Zhang Nan, Wang Miaohui, Zhang Fuyan *et al*. *Rare Metal Materials and Engineering*[J], 2022, 51(7): 2698 (in Chinese)

fcc高熵合金变形机制的中子衍射研究进展

赵燕春[1]，姚亚桃[1,2,3,4]，张　凡[4]，黄　燕[4]，张艺波[4]，吕志超[4]，张　琪[4]，付小玲[5]，王安定[6]，张　飞[2]，宋温丽[2,3]，马　东[4]

(1. 兰州理工大学 材料科学与工程学院 省部共建有色金属先进加工与再利用国家重点实验室，甘肃 兰州 730050)
(2. 中国科学院 高能物理研究所，北京 100049)
(3. 散裂中子源科学中心，广东 东莞 523803)
(4. 松山湖材料实验室 中子科学中心，广东 东莞 523808)
(5. 广东工业大学 材料与能源学院，广东 广州 510006)
(6. 东莞理工学院 材料科学与工程学院 交叉科学研究中心，广东 东莞 523808)

摘　要：高熵合金的“多主元”特性，颠覆了传统“单一主元”的合金设计理念，使其具有优异的力学性能。然而，也正因为“多主元”，高熵合金具有复杂的变形行为，表现为多种变形机制交替出现且耦合关联。因此，厘清高熵合金的复杂变形机制是当前研究的难点。在表征复杂变形行为方面，中子衍射技术比传统显微方法更具优势，其强穿透性可原位、实时、无损探测厘米级块体样品在复杂环境下的结构演变，且中子衍射可精确表征C、O等轻元素和近邻元素的晶胞占位。本文从中子衍射原理、实验及数据分析出发，结合当前面心立方高熵合金研究的最新进展，总结并展示了运用中子衍射探究其变形行为的典型范例，揭示了位错、层错、孪晶和相变主导的变形机制。

关键词：高熵合金；中子衍射；面心立方结构；变形机制

作者简介：赵燕春，女，1984年生，博士，教授，兰州理工大学材料科学与工程学院省部共建有色金属先进加工与再利用国家重点实验室，甘肃 兰州 730050，E-mail：zhaoyanchun@edu.lut.cn